Conservation of an immune homeostasis module in land plants

Ruoqi Dou[1], Karima El Mahboubi[2], Cailun A.S. Tanney[1], Jiashu Chu[3,a], Melissa Bredow[1], Maria Camila Rodriguez Gallo[4], Dominique Lauressergues[2], Jean Keller[2], Virginia Natali Miguel[1], Thomas A. DeFalco[3,b], R. Glen Uhrig[4,5], Cyril Zipfel[3,6], Pierre-Marc Delaux[2], and Jacqueline Monaghan[1,*]

[1] Department of Biology, Queen's University, Kingston, ON, Canada.

[2] Laboratoire de Recherche en Sciences Végétales (LRSV), Université de Toulouse, CNRS, UPS, Toulouse INP, Castanet-Tolosan, France.

[3] Institute of Plant and Microbial Biology and Zurich-Basel Plant Science Center, University of Zurich, Zurich, Switzerland.

[4] Department of Biological Sciences, University of Alberta, Edmonton, AB, Canada.

[5] Department of Biochemistry, University of Alberta, Edmonton, AB, Canada.

[6] The Sainsbury Laboratory, University of East Anglia, Norwich Research Park, Norwich, United Kingdom.

*Lead contact: jacqueline.monaghan@queensu.ca

[a] Present address: Laboratory of Biochemistry, Wageningen University, Wageningen, the Netherlands

[b] Present address: Department of Biology, Western University, London, ON, Canada

24 # ORCiDs

Author	ORCiD
Ruoqi Dou	0009-0000-3266-9233
Karima El Mahboubi	0009-0006-1199-5500
Jiashu Chu	0009-0008-7651-1102
Melissa Bredow	0000-0002-5564-9646
Maria Camila Rodriguez Gallo	0000-0003-2171-6158
Dominique Lauressergues	0000-0003-0420-2366
Jean Keller	0000-0002-5198-0331
Virginia Natali Miguel	0009-0008-9546-6677
Thomas DeFalco	0000-0003-2897-1485
R. Glen Uhrig	0000-0003-2773-4381
Cyril Zipfel	0000-0003-4935-8583
Pierre-Marc Delaux	0000-0002-6211-157X
Jacqueline Monaghan	0000-0002-1770-1669

25

Highlights

- MpCPK28 is a Ca^{2+}-dependent protein kinase that regulates immune homeostasis and development in Marchantia and is functionally orthologous to AtCPK28.
- MpCPK28 phosphorylates the E3 ubiquitin ligase MpPUB20e and the receptor-like cytoplasmic kinase MpPBLa.
- MpPBLa is subject to proteasomal degradation and is ubiquitinated by MpPUB20e.

In Brief

Deploying robust immune responses to deter pathogens while minimizing host damage is critical to plant survival. Here, Dou *et al*. show that optimizing the protein accumulation of receptor-like cytoplasmic kinase MpPBLa is an ancient property of the plant immune system, controlled by the MpCPK28-MpPUB20e regulatory module.

Summary

Calcium-dependent protein kinases (CDPKs or CPKs) are a unique family of Ca^{2+}-regulated kinases with diverse functions in plants [1]. CPK28 regulates immune homeostasis, stress responses, and growth in multiple angiosperms including tomato [2,3], rice [4–7], cotton [8–10], and *Arabidopsis thaliana* (hereafter, Arabidopsis)[11–17]. In Arabidopsis, CPK28 phosphorylates and activates the E3 ubiquitin ligases PLANT U-BOX 25 (PUB25) and PUB26 that target the major immune signaling protein BOTRYTIS-INDUCED KINASE 1 (BIK1), resulting in its turnover [12,18]. The CPK28-PUB25/26-BIK1 regulatory module maintains precise levels of BIK1 in the cell and is thought to optimize immune responses [19]. Separated from angiosperms by 450M years of evolution, the liverwort *Marchantia polymorpha* (hereafter, Marchantia) has emerged as a model system to study the evolution of signaling modules across land plants [20]. Here, we demonstrate that the

51 function of CPK28 is conserved in Marchantia. MpCPK28 displays Ca^{2+}-dependent
52 protein kinase activity and is inhibited by calmodulin *in vitro*. Over-expression of
53 *MpCPK28* results in pronounced developmental phenotypes and decreased chitin-
54 induced oxidative burst, and *MpCPK28* can functionally complement the mutant
55 phenotypes of the Arabidopsis *cpk28-1* mutant. MpCPK28 associates with and
56 phosphorylates multiple residues on Marchantia AVRPPHB SUSCEPTIBLE 1 (PBS1)-
57 like (PBL)-a (MpPBLa), a functional ortholog of AtBIK1, as well as MpPUB20e (a putative
58 ortholog of AtPUB25/26). MpPBLa undergoes proteasomal degradation in Marchantia
59 and can be polyubiquitinated by MpPUB20e. The occurrence of the CPK28-PUB25/26-
60 BIK1 module across land plants reveals that the regulation of immune amplitude has been
61 conserved throughout plant evolution.

62

63 Results and Discussion

64 MpCPK28 regulates immune homeostasis and development in Marchantia

65 Calcium-dependent protein kinases (CDPKs) are a unique family of Ca^{2+}-regulated
66 kinases found in apicomplexan protists [21], red and green algae [22,23], and throughout the
67 plant kingdom [1,23]. Following divergence from a common ancestor, CDPKs in the plant
68 kingdom separated into five phylogenetic subgroups (I, II, III, IV, and CDPK-related
69 proteins, CRKs) [1,23,24]. This diversification occurred between 270-340 MYA [23], which is
70 after terrestrial habitation (~400-700 MYA) and coincides with the transition from
71 nonvascular to vascular plants (~350-400 MYA). It is noteworthy that CDPKs in
72 Charophyte algae (including *Klebsormidium nitens, Chara braunni,* and *Spirogloea*
73 *muscicola*) and nonvascular plants (including Marchantia*, Selaginella moellendorffii,* and
74 *Physcomitrium patens*) cluster into the subgroups but are basal to angiosperm CDPKs
75 (**Figures 1A; S1**). This evolutionary history suggests that expansion of the CDPK family
76 may have played a role in adapting to life on land [23]; something that is also supported by

77 the diverse roles played by CDPKs in developmental programs and stress responses in
78 angiosperm models such as Arabidopsis and *Oryza sativa* (hereafter, rice) [1].

79 The first divergence from the last common CDPK ancestor appears to be
80 subgroups IV and CRK [23] (**Figures 1A; S1)**. To investigate the deep evolutionary history
81 of subgroup-IV CDPKs, we analyzed sequences from 193 genomes across all major plant
82 lineages (**Figure S2**). Although some variations in protein domain organization can be
83 observed (**Figure S2**), subgroup-IV CDPKs are highly conserved across land plants. In
84 several instances, lineage- and/or species-level duplications resulted in co-orthologs; for
85 example the three co-orthologs in Arabidopsis (AtCPK16, AtCPK18, and AtCPK28)
86 emerged from a Brassicaceae-specific triplication. The subgroup-IV CDPK CPK28 is a
87 major regulator of immune homeostasis and growth in multiple angiosperms including
88 tomato [2,3], rice [4–7], cotton [8–10], and Arabidopsis [11–13,15,16,25–28]. In addition, AtCPK16 may
89 also play a role in defense against bacterial and viral infections [29]. Despite this abundance
90 of evidence supporting key roles for subgroup-IV CDPKs in immune optimization in
91 angiosperms, it is not clear if this is an ancient property of this gene family. We took
92 advantage of recent advances in functional genomics in the nonvascular plants
93 *Marchantia polymorpha* and *M. palaceae* to address this question.

94 We identified a single subgroup-IV CDPK in Marchantia:
95 Mp4g01600/Mapoly0098s0040/Mar_contig_10180 (hereafter, MpCPK28) (**Figures 1A;**
96 **S1; S2; S3A**) that is broadly expressed in both the thallus and sexual reproductive tissues
97 (**Figure S3B**). Loss-of-function *cpk28* mutants in Arabidopsis [12,15], rice [4], cotton [8,10], and
98 tomato [3], display enhanced immune signaling and anti-microbial resistance.
99 Overexpression of AtCPK28 confers strongly reduced immune responses in Arabidopsis
100 [12]. To test the function of MpCPK28 in Marchantia, we generated multiple MpCPK28
101 overexpression lines. However, only one, MpCPK28-OE2, was capable of producing
102 viable gemmae. We confirmed that *MpCPK28* is expressed ~30X higher in thallus tissue
103 of MpCPK28-OE2 compared to wild-type accession Tak-1 (**Figure S3C**), allowing us to
104 carry out functional studies.

105 Chitin, a key component of fungal and insect cell walls, displays immunogenic
106 properties across land plants and is recognized in Marchantia by the LysM-receptor
107 kinases MpLYK1 and MpLYR [30]. In angiosperms, subgroup-VII receptor-like cytoplasmic
108 kinases (RLCKs) are activated immediately following immune detection, enabling them
109 to phosphorylate a myriad of targets to propagate signaling [31]. In Marchantia, the
110 subgroup-VII RLCK MpPBLa is phosphorylated at its N-terminus following chitin
111 treatment [30] and is genetically required for chitin signaling [32]. We add that when expressed
112 heterologously in *Nicotiana benthamiana*, MpPBLa-GFP localizes to the plasma
113 membrane (**Figure S4**). A conserved hallmark of immune induction in plants is a rapid
114 burst of apoplastic reactive oxygen species (ROS) [30–32]. Functionally orthologous to
115 AtBIK1 [33], MpPBLa directly phosphorylates conserved N-terminal residues on the
116 NADPH oxidase MpRBOH1 required for its function [32]. We observed significantly lower
117 chitin-induced ROS in MpCPK28-OE2 compared to Tak-1 (**Figure 1B-C**), indicating that
118 MpCPK28 plays a role in optimizing ROS production and suggesting that MpCPK28
119 functions as part of the Marchantia immune system. The MpCPK28-OE2 line additionally
120 displayed defects in both gemmae and thallus morphology. Whereas Tak-1 gemmae
121 have two distinct apical notches (meristems), the majority (67%) of MpCPK28-OE2
122 gemmae appear to have several (**Figure 1D; S3D**). Notably, the number of apical notches
123 in MpCPK28-OE2 is highly variable, fluctuating between 3-10 with irregular distribution
124 (**Figure 1D**). This atypical gemmae morphology is reflected in thallus development, which
125 appears highly disordered compared to Tak-1 (**Figure 1E**). These results indicate that
126 overexpression of MpCPK28 disrupts developmental programs and suggest a role for
127 MpCPK28 in cell division and apical notch differentiation. We conclude that MpCPK28
128 functions in multiple pathways in Marchantia, including immune and developmental
129 signaling.

130

131 ## MpCPK28 is a Ca^{2+}-dependent protein kinase inhibited by calmodulin

132 As protein kinases, CDPKs phosphorylate targets to affect their function, localization, or
133 binding partners. Thought to have evolved from the ancestral fusion between calmodulin
134 (CaM) and CaM kinase (CaMK) [34], CDPKs contain both an N-terminal kinase domain and
135 a C-terminal CaM-like domain. In between those domains is an auto-inhibitory junction
136 (AIJ) that plays an important structural role in activation. Acting like the hinge of a gate,
137 the AIJ inhibits the active site of the kinase domain when in its 'off' state, but swings open
138 when Ca^{2+} is bound to the CaM-like domain in its 'on' state. AtCPK28 has a low threshold
139 for activation by Ca^{2+} and displays high activity *in vitro* even without the addition of Ca^{2+}
140 [11,26,35]. However, activity is reduced when Ca^{2+} ions are chelated with EGTA [11,26,35],
141 indicating that AtCPK28 is indeed Ca^{2+}-dependent. We similarly found that His_6-
142 MpCPK28 displays Ca^{2+}-dependent kinase activity with a low threshold for activation *in*
143 *vitro* (**Figure 1F**). Within the AIJ is the CaM-binding domain (CBD), which is the site for
144 intramolecular interaction with the C-terminal CaM-like domain [36]. AtCPK28 also forms
145 Ca^{2+}-dependent interactions with exogenous CaM, something that is unique amongst the
146 AtCDPK family [35]. This intermolecular interaction occurs via the CBD and is regulated by
147 autophosphorylation on Ser360 [35]. Because the CBD in subgroup-IV CDPKs is highly
148 conserved across land plants (**Figure 1G**), we tested if MpCPK28 activity can also be
149 inhibited by CaM *in vitro* and found this was indeed the case (**Figure 1H**). We conclude
150 that MpCPK28 is a Ca^{2+}-dependent protein kinase that can be inhibited by CaM, which
151 may reflect a general property of subgroup-IV CDPKs.

152

153 ## MpCPK28 complements Arabidopsis *cpk28-1* mutants

154 To assess whether the molecular function of CPK28 is conserved between *M.*
155 *polymorpha* and angiosperms, we transformed Arabidopsis *cpk28-1* mutants with
156 MpCPK28 C-terminally tagged with green fluorescent protein (GFP) driven by the
157 cauliflower mosaic virus (CaMV) *35S* promoter. We additionally transformed *cpk28-1*
158 plants with the mutant variant $MpCPK28^{K128E}$ that is predicted to be catalytically inactive

159 due to the loss of a critical lysine in the ATP-binding site. We isolated homozygous
160 transgenic lines and confirmed expression of the recombinant proteins by immunoblot
161 (**Figure S5**). Notably, the wild-type protein displayed a higher molecular weight compared
162 to the catalytically inactive variant, suggesting that MpCPK28 autophosphorylates *in*
163 *planta*, similar to AtCPK28 [11]. Also similar to AtCPK28-YFP [12], both MpCPK28-GFP and
164 MpCPK28^{K128E}-GFP localize to the plasma membrane (**Figure 2A**). Mutant *cpk28-1*
165 plants display both enhanced immune signaling [12] as well as defects in stem elongation
166 [11]. While MpCPK28-GFP complemented the stem elongation defect in *cpk28-1*, the
167 catalytically inactive variant did not (**Figure 2B**). This suggests that MpCPK28 is able to
168 replace AtCPK28 during the vegetative-to-reproductive stage transition in a kinase
169 activity-dependent manner. Likewise, MpCPK28, but not MpCPK28^{K128E}, is also able to
170 complement enhanced immune-triggered ROS burst (**Figure 2C**) and seedling growth
171 inhibition (**Figure 2D**) in *cpk28-1*. We conclude that the molecular function of CPK28 has
172 been conserved across land plants.

173

174 MpCPK28 phosphorylates MpPUB20e and MpPBLa

175 In Arabidopsis, AtCPK28 phosphorylates two related E3 ubiquitin ligases, AtPUB25 and
176 AtPUB26, contributing to their activation and subsequent poly-ubiquitination of
177 unactivated AtBIK1, resulting in its proteasomal degradation [18]. It is thought that this limits
178 AtBIK1 availability to optimize immune signaling [12,18]. AtPUB25/26 are part of the large
179 subgroup IV of plant U-box (PUB) proteins that contain an N-terminal U-box domain and
180 a C-terminal Armadillo (ARM) repeat domain [18,37]. A recent phylogeny of the PUB family
181 across land plants indicates the presence of 38 PUB genes in Marchantia (MpPUBs), of
182 which 11 belong to subgroup IV [37]. Whilst none of the MpPUBs form a monophyletic group
183 with AtPUB25/26 or related AtPUB22/23/24, seven are basal to the sister group
184 AtPUB20/21 which we name MpPUB20a-g (sharing 30-70% amino acid sequence
185 identity) (**Figure S6A**). Notably, *pub20 pub21* double mutants, *pub22 pub23 pub24* triple
186 mutants, and *pub25 pub26* double mutants all display enhanced immune signaling in

187 Arabidopsis, and there is functional redundancy in this gene family [18,38,39]. Based on their
188 phylogenetic relationship and gene expression profiles (**Figure S6B**), we chose five
189 MpPUBs to test as putative MpCPK28 substrates: MpPUB20a/Mp3g01700,
190 MpPUB20c/Mp3g22740, MpPUB20d/Mp3g11730, MpPUB20e/Mp7g11020, and
191 MpPUB20g/Mp7g11000. Of these, MpCPK28 readily phosphorylated MpPUB20e *in vitro*
192 (**Figure 3A**). Using mass spectrometry, we identified four residues that are
193 phosphorylated by MpCPK28 *in vitro*: Ser16, Ser19, and Ser21 at the far N-terminus, and
194 Ser159 at the start of the U-box domain (**Figure 3B**). Although no chitin-induced
195 phosphopeptides matching MpPUB20e were identified in a previous study [30], AtPUB26
196 is phosphorylated on eight residues following treatment with the bacterial immune elicitor
197 flg22 [18], including Ser120 which is orthologous to MpPUB20e-Ser159, as well as Thr94
198 located in the region between the U-box and ARM repeats (**Figure 3C**). Whilst the
199 function of AtPUB26-Ser159 is unknown, both AtPUB26-Thr94 and the conserved site
200 Thr95 on AtPUB25 were shown to be phosphorylated by AtCPK28 *in vitro,* as detected
201 by anti-pThr95/94 immunoblot, and phosphorylation of AtPUB25/26-Thr95/94 contributes
202 to its catalytic activity [18]. Furthermore, immune-triggered phosphorylation of the
203 conserved site Thr88 on AtPUB22 also regulates its function [40]. Overall, our results
204 indicate that both MpCPK28 and AtCPK28 phosphorylate MpPUB20e or AtPUB25/26 in
205 at least one conserved position, suggesting that this regulatory unit is ancient.

206 AtCPK28 also directly phosphorylates AtBIK1, which is hypothesized to impact its
207 degradation [12]. Similarly, rice OsCPK4 phosphorylates OsRLCK176 [4,41] and cotton
208 (*Gossypium hirsutum*) GhCDPK28 interacts with GhPBL9 [8], suggesting that this
209 interaction is functionally conserved in angiosperms. Moreover, MpPBLa, AtBIK1,
210 OsRLCK176 are all critical regulators of immune signaling in Marchantia, Arabidopsis,
211 and rice, respectively [32,42–46]. *In vitro* kinase assays indicate that His_6-MpCPK28 is
212 capable of phosphorylating the catalytically inactive variant MBP-MpPBLa^{D228N} (**Figure**
213 **3D**). Using mass spectrometry, we identified six sites that are phosphorylated by
214 MpCPK28 *in vitro*, four of which (Ser43, Ser45, Ser46, and Ser70) are located in the
215 intrinsically disordered N-terminal region of MpPBLa (**Figure 3E**). Notably, a

216 phosphopeptide including Ser70 was found to be induced by chitin in a previous study,
217 and phosphopeptides including Ser43, Ser45, and Ser46 were identified in untreated
218 samples [30], suggesting a role for phosphorylation-mediated regulation at the N-terminus
219 of MpPBLa. OsCPK4 can phosphorylate seven residues on OsRLCK176, with a
220 preference for Ser74 in the N-terminal disordered region and Ser209, Ser267, and Ser336
221 in the kinase domain [4]. Together these results suggest that CPK28 orthologs
222 phosphorylate the N-termini of BIK1 orthologs in Arabidopsis, rice, and Marchantia.
223 Phosphorylation of intrinsically disordered regions is known to regulate protein function
224 [47], and it will be of interest to explore how the N-terminal variable regions of RLCKs
225 contribute to their function. Overall, we conclude that both MpPUB20e and MpPBLa are
226 substrates of MpCPK28, suggesting that the CPK28-PUB25/26-BIK1 module is
227 conserved and ancient in land plants.

228

229 MpPBLa is subject to proteasomal turnover and is ubiquitinated by 230 MpPUB20e *in vitro*

231 To assess if MpPBLa is subject to proteasomal degradation, we performed cell-free
232 degradation assays with or without proteasome inhibitor MG132. We found that both
233 MBP-MpPBLa and GST-AtBIK1 undergo proteasomal degradation when incubated in
234 either Tak-1 (**Figure 4A,B**) or Col-0 (**Figure S7A,B**) protein extract, indicating that
235 Marchantia and Arabidopsis possess conserved machinery capable of degrading
236 MpPBLa and AtBIK1. We next aimed to test if MpPUB20e is able to ubiquitinate MpPBLa.
237 We first assessed if MpPUB20e is an active E3 ubiquitin ligase. Previous work indicated
238 that AtPUB22 can interact with several subgroup-VI E2 ubiquitin conjugating enzymes
239 (UBCs) [48], and that AtPUB25/26 can pair with AtUBC8 [18]. We thus used subgroup VI E2s
240 AtUBC8 and AtUBC30 (which share 96% and 85% amino acid sequence identity to
241 Marchantia UBC protein Mp5g21800, respectively) in our assays. We found that
242 MpPUB20e is able to auto-polyubiquitinate when paired with either AtUBC8 or AtUBC30
243 (**Figure S8**), indicating that it possesses catalytic activity *in vitro*. Whilst we were unable

244 to detect polyubiquitination by MpPUB20e-AtUBC8 on MpPBLa (**Figure 4C**), we were
245 able to detect polyubiquitination on the catalytically inactive mutant MpPBLa^{D228N} (**Figure**
246 **4D**). This is notable since AtPUB25/26 preferentially polyubiquitinate inactive AtBIK1 in
247 Arabidopsis [18], and suggests that MpPUB20e also preferentially targets inactive MpPBLa.
248 Together, these results suggest that MpPBLa is under proteasomal control and that
249 optimization of protein accumulation is a conserved feature of MpPBLa/AtBIK1 across
250 land plants (**Figure 4E**).

251

252 Conclusion

253 Our results suggest that safeguarding immune signaling is an ancient property of the plant
254 immune system. We show that MpPBLa protein accumulation is controlled by MpCPK28
255 and MpPUB20e in Marchantia, indicating that this regulatory module has been conserved
256 for at least 450 MY in plants with vastly different life history and developmental traits that
257 engage with unique microbial populations.

258

259 Acknowledgements

260 We thank all members of the Monaghan Lab for their commitment to fostering a
261 welcoming and collaborative research environment. Queen's University is situated on the
262 territory of the Haudenosaunee and Anishinaabek and we are grateful to live, work, and
263 play on these lands. We are grateful to all members of our labs, past and present, for
264 engaging discussions over the course of this project, and for reviewing our manuscript
265 before submission. We thank Dale Kristensen and Saeid Mobini for managing the
266 Queen's University Phytotron Facility; Tony Papanicolaou for managing the Queen's
267 University Department of Biology Microscopy Suite; Jack Moore for technical assistance
268 and maintenance of the University of Alberta Mass Spectrometry and Proteomics Facility;
269 Anamika Rawat for training assistance in confocal microscopy; Brandon Saltzman for

preliminary work on the MpPUB phylogeny; Katherine Dunning for establishing the cell-free degradation assay in our lab; and Kathy Sihavong for assisting with cloning MpCPK28. This work was funded by grants awarded to **JM**: Canadian Natural Sciences and Engineering Research Council of Canada (NSERC) Discovery and Discovery Accelerator Programs (RGPIN-2016-04787, RGPAS-492902-2016, and RGPIN-2024-04072), the Canada Research Chair (CRC) Program, and Queen's University; as well as grants awarded to **PMD**: Labex TULIP (ANR-10-LABX-41), the project Engineering Nitrogen Symbiosis for Africa (ENSA) currently funded through a grant to the University of Cambridge by the Bill and Melinda Gates Foundation (OPP1172165) and the UK Foreign, Commonwealth and Development Office as Engineering Nitrogen Symbiosis for Africa (OPP1172165); grants to **CZ**: Swiss National Science Foundation (grant agreement no. 31003A_182625), Gatsby Charitable Foundation, and the University of Zurich; and grants to **RGU**: the Canadian Foundation for Innovation (CFI) John R. Evans Leaders Fund (JELF; grants 41831 and 37833). **MB** was supported by an NSERC Postdoctoral Fellowship (2019-2021). **TAD** was supported by a Long-Term Fellowship from the European Molecular Biology Organization (2017-2019) and an NSERC Postdoctoral Fellowship (2019-2021). **MCRG** was supported by an Alberta Graduate Excellence Scholarship (AGES).

Author Contributions

JM and **PMD** conceived and designed the project. **RD**, **KEM**, **CAST**, **JC**, **MB**, **MCRG**, **DL**, **JM** generated materials, performed experiments, and/or analyzed data. **JK** and **VNM** performed phylogenetics. **JM**, **PMD**, **RGU**, **TAD**, **CZ** supervised the project. **JM** wrote the manuscript with input from all authors.

Declarations of interest

The authors declare no conflicts of interest.

Figures

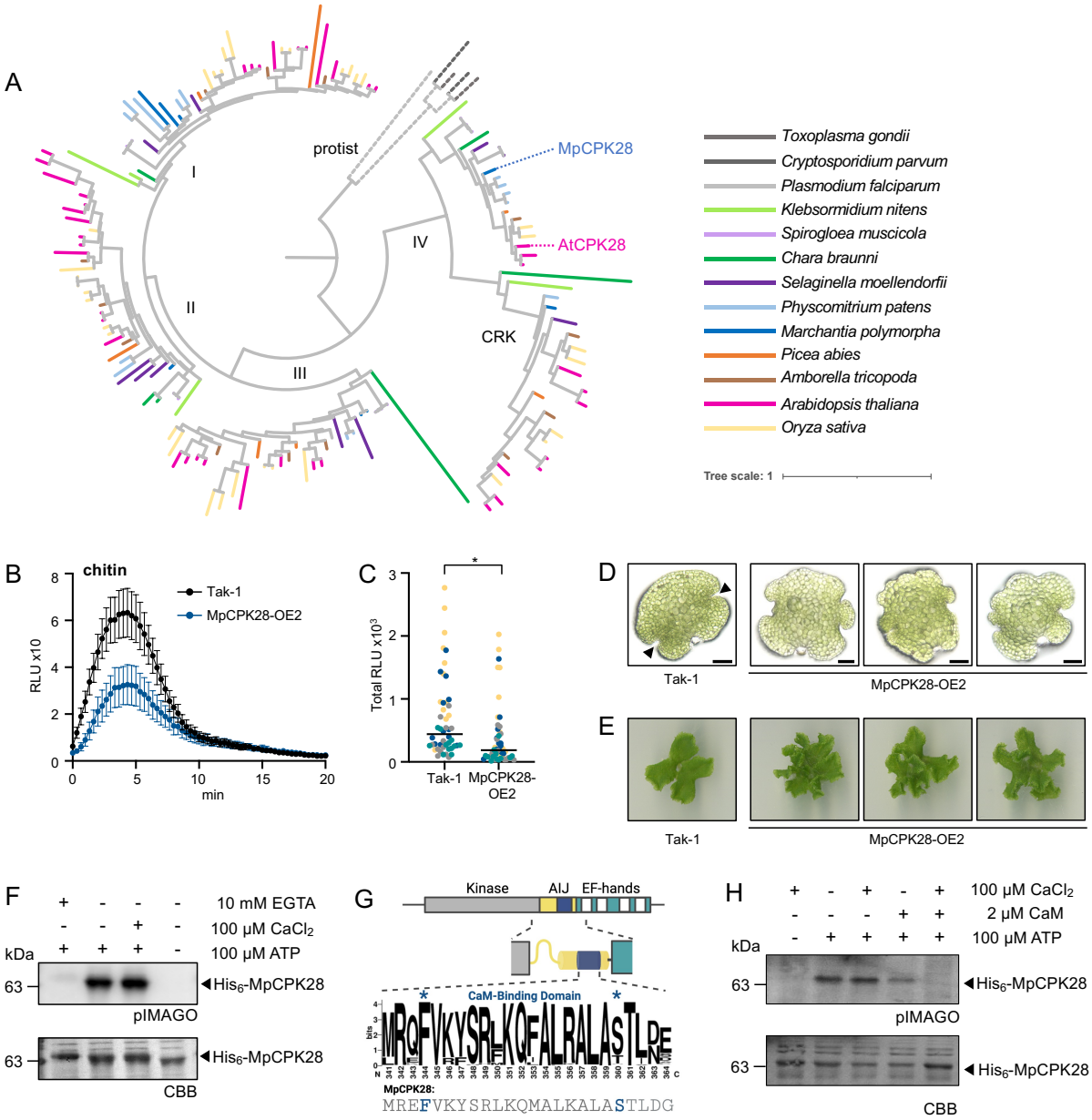

Figure 1. MpCPK28 regulates chitin-induced ROS production and development in Marchantia.

(A) Phylogenetic tree of CDPKs from various plant lineages, with subgroups I, II, III, IV, and CRK indicated. The tree was constructed using the Maximum Likelihood method with IQ-TREE v2.3.4 (1,000 SH-aLRT and ultraFast bootstrap replicates) and Jackknife resampling. A total of 157 CDPK protein sequences from *Selaginella moellendorffii, Physcomitrium patens, Chara braunii, Klebsormidium nitens, Spirogloea*

303 *muscicola, Oryza sativa, Amborella tricopoda, Picea abies, Arabidopsis thaliana* and *Marchantia*
304 *polymorpha* were aligned with MAFFT v7.490, trimmed using TrimAL v1.4.rev15, and visualized in iTOL.
305 Five apicomplexan CDPK sequences were used as an outgroup. See **Figure S1** for a fully labeled tree.
306 Phylogenetic analysis by VNM, visualized in iTOL. **(B-C)** ROS production measured in relative light units
307 (RLUs) after treatment with 0.1 mg/mL chitin. Values in **B** represent means +/- standard error (n=12 thallus
308 discs) over a 20-min time-course from one representative experiment; values in **C** represent total RLU
309 observed for each genotype, colour-coded by experimental replicate (n=4 replicates of 12 thallus discs
310 each). Asterisk indicates a statistically significant difference between the indicated genotypes (unpaired
311 Student's t-test; p=0.0118). Assays were repeated four times by JC. **(D)** Gemma from the indicated
312 genotypes observed under a light microscope. Typical apical nodes are indicated by black arrowheads on
313 Tak-1. Scale bar: 100 μm. **(E)** Representative thalli from 1-month-old plants of the indicated genotypes.
314 Similar morphology was observed in **D** and **E** over several years by KEM. **(F)** *In vitro* kinase assays of His_6-
315 MpCPK28 with and without EGTA, $CaCl_2$, or ATP, visualized using pIMAGO. Coomassie Brilliant Blue
316 (CBB) indicates loading. These experiments were repeated several times with similar results by MB and
317 RD; representative blots by MB are shown. **(G)** Schematic indicating the location of the CaM-binding
318 domain (coloured blue) within the autoinhibitory junction (AIJ; coloured yellow) of a canonical CDPK.
319 WebLogo indicates conservation within this region in subgroup IV CDPKs from 53 species (described in
320 [26]). The specific sequence of this region in MpCPK28 is shown below the logo. Asterisks indicate residues
321 shown to be important for CaM binding in AtCPK28 [35]. This figure was created in BioRender by JM. **(H)** *In*
322 *vitro* kinase assays of His_6-MpCPK28 with and without CaM, $CaCl_2$, or ATP, visualized using pIMAGO.
323 Coomassie Brilliant Blue (CBB) indicates loading. These experiments were repeated several times with
324 similar results by RD; representative blots are shown. Cloning credits are provided in **Table S1**.

325

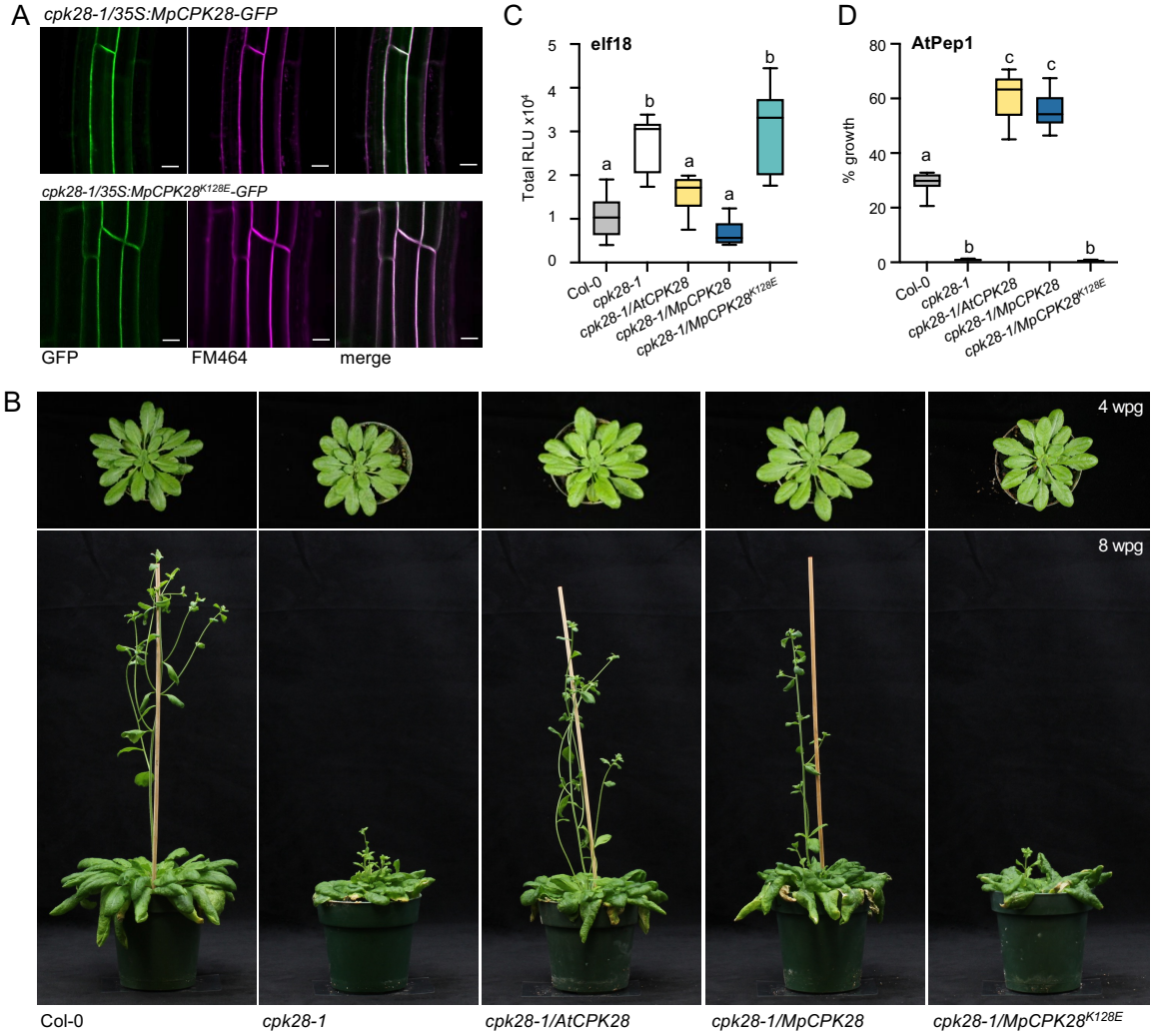

Figure 2. MpCPK28 complements Arabidopsis *cpk28-1* mutants.

(A) Single-plane confocal micrographs of root cells from the indicated genotypes indicating the subcellular localization of MpCPK28-GFP and MpCPK28^{K128E}-GFP (GFP) and the plasma membrane (FM464). Scale bar indicates 10 µm. **(B)** Photos of Arabidopsis plants at 4 (upper) and 8 (lower) weeks post germination (wpg) grown under short-day conditions. **(C)** ROS production measured in relative light units (RLUs) after treatment with 200 nM elf18. Values represent total RLU observed for each genotype (n=6 leaf discs from different plants), displayed as boxplots indicating first and third quartiles, split by a median line. Whiskers represent maximum and minimum values. Statistically significant groups were evaluated by a one-way ANOVA followed by a Tukey's post-hoc test and are indicated by lower-case letters ($p<0.05$). **(D)** Seedling growth inhibition assay indicating % growth in media containing 500 nM AtPep1 peptide relative to growth in media without peptide. Values represent % fresh weight of single seedlings (n=8 for each treatment per genotype), displayed as boxplots in the same way as in **C**. Statistically significant groups were evaluated by a one-way ANOVA followed by a Tukey's post-hoc test and are indicated by lower-case letters ($p<0.0001$). Similar observations were made across generations over multiple years by RD, CAST, and MB; representative data collected by RD are shown. Details regarding plant genotypes are provided in **Table S1**.

343

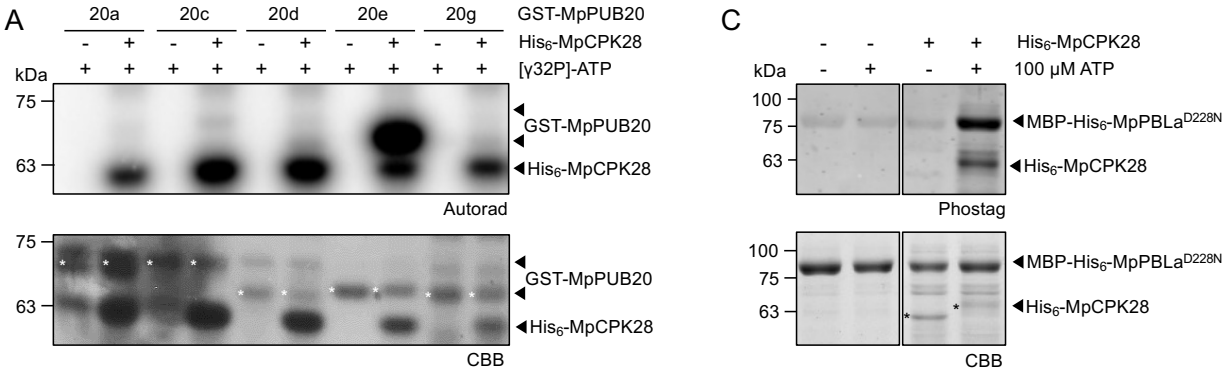

B

MpPUB20e phophopeptide	Residue	Location
LE**[pS]**GH[pS]LSR	S16	
LE[pS]GH**[pS]**LSR	S19	N-terminus
VSRLESGHSL**[pS]**R	S21	
GLATE**[pS]**DRNMR	S159	U-box

D

MpPBLa phophopeptide	Residue	Location
PGPTK**[pS]**GSTDFSNSGGDLPDVTPR	S43	
SG**[pS]**TDFSNSGGDLPDVTPR	S45	N-terminus
SGS**[pT]**DFSNSGGDLPDVTPR	T46	
IALPTVDD**[pS]**VR	S70	
DGPEGDKTHV**[pS]**TR	S262	Activation loop
LDNQY**[pS]**LR	S343	Kinase C-lobe

344

345 Figure 3. MpCPK28 phosphorylates MpPUB20e and MpPBLa.

346 **(A)** *In vitro* kinase assays using His_6-CPK28 as the kinase and GST-tagged MpPUB20a ('20a'), MpPUB20c
347 ('20c'), MpPUB20d ('20d'), MpPUB20e ('20e'), or MpPUB20g ('20g') as substrates. Autoradiographs
348 (autorad) indicate incorporation of γ32P and protein loading is indicated by post-staining with Coomassie
349 Brilliant Blue (CBB). Assays were performed more than 3 times each by RD with similar results;
350 representative data are shown. **(B)** Unique MpPUB20e phosphopeptides following kinase assays with His_6-
351 CPK28. Each peptide was present in at least 2/3 independent replicates and not found in control samples
352 with ATP but without His_6-CPK28. The bolded sites are the phosphosites and their positions are indicated
353 on the right. Kinase assays performed by RD; trypsin digests and LC-MS/MS performed by MCRG. **(C)** *In*
354 *vitro* kinase assays using His_6-CPK28 as the kinase and catalytically inactive MBP-His_6-MpPBLa^{D228N} as
355 the substrate, visualized using Phostag gel staining. Coomassie Brilliant Blue (CBB) indicates loading.
356 These experiments were repeated more than four times by RD and MB over several years and
357 representative blots by RD are shown. **(D)** Unique MpPBLa phosphopeptides following kinase assays
358 between His_6-CPK28 and MBP-His_6-MpPBLa^{D228N}. Each peptide was present in at least 2/3 independent
359 replicates and not found in control samples with ATP but without His_6-CPK28. The bolded sites are the
360 phosphosites and their positions are indicated on the right. Kinase assays performed by RD; trypsin digests
361 and LC-MS/MS performed by MCRG. Cloning credits are provided in **Table S1**.

362

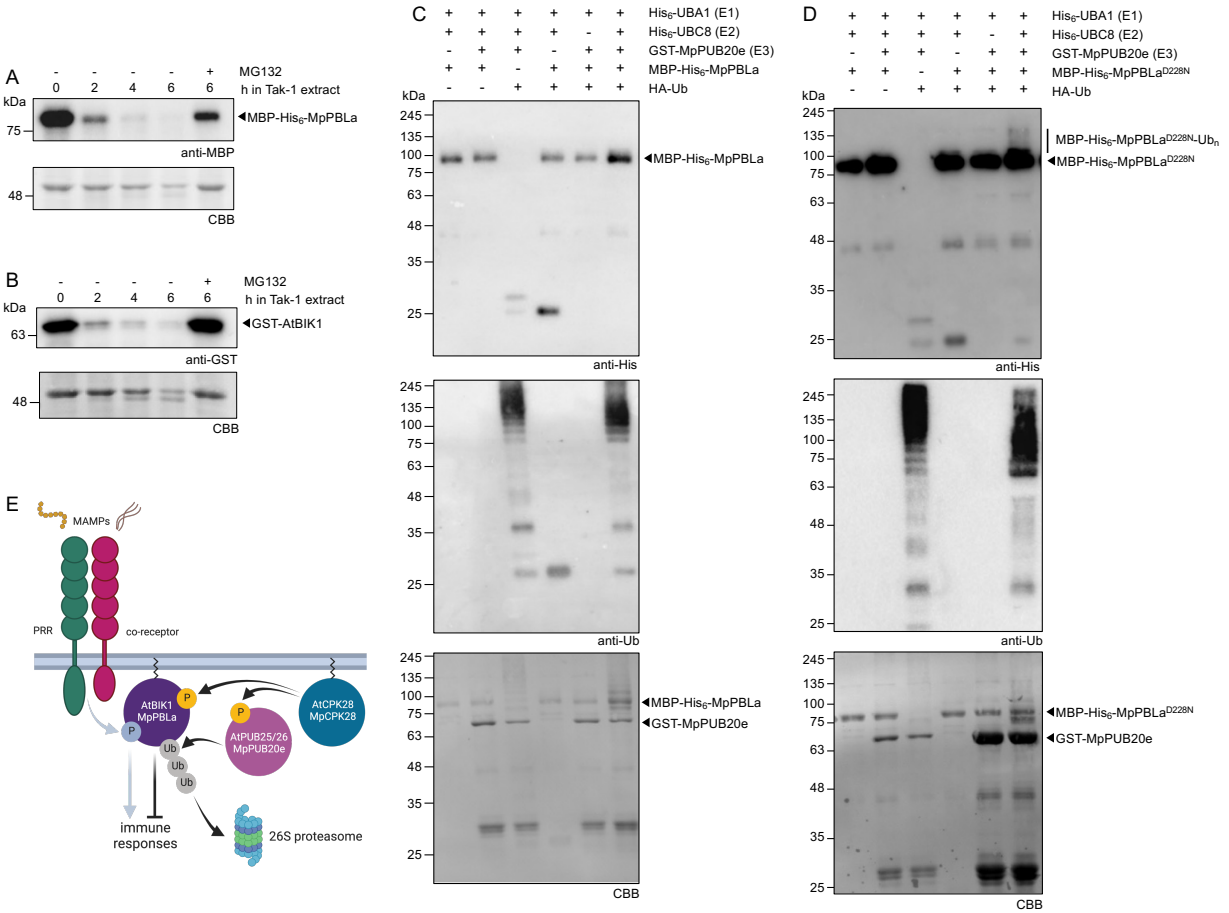

363

364 Figure 4. MpPBLa is subject to proteasomal turnover and is ubiquitinated by
365 MpPUB20e *in vitro.*

366 **(A-B)** Degradation of recombinant MBP-His$_6$-MpPBLa **(A)** or GST-AtBIK1 **(B)** following incubation for 0, 2,
367 4, or 6 hours in total protein extract from Marchantia Tak-1 tissue with or without the proteasome inhibitor
368 MG132. Western blots were probed with either anti-MBP or anti-GST antibodies, and protein loading is
369 indicated by post-staining of Coomassie Brilliant Blue (CBB) of RuBisCO. **(C-D)** *In vitro* ubiquitination
370 assays using His$_6$-AtUBC1 as the E1 activating enzyme, His$_6$-AtUBC8 as the E2 conjugating enzyme, GST-
371 MpPUB20e as the E3 ligase enzyme, and either MBP-His$_6$-MpPBLa **(C)** or MBP-His$_6$-MpPBLa^{D228N} **(D)** as
372 substrate. The upper western blots are probed with anti-His; the middle blot is probed with anti-Ub; and
373 protein loading is indicated by post-staining with Coomassie Brilliant Blue (CBB). These assays were
374 repeated more than three times with similar results by RD. Cloning credits are provided in **Table S1**. **(E)**
375 Model indicating conservation of the CPK28-PUB25/26-BIK1 module in Arabidopsis and Marchantia. This
376 figure was created in BioRender by MB and JM.

377

378

379 # Star Methods

380 ## Key Resources Table

Reagent or Resource	Source	Identifier
Antibodies		
Mouse anti-His (27E8)	Cell Signaling	2366S
Rabbit anti-Streptavidin	Sigma	S6390
Mouse anti-GFP	Roche	11814460001
Mouse anti-GST	Sigma	SAB4200237
Mouse anti-MBP	New England Biolabs	E8032S
Mouse anti-Ub (P4D1)	Cell Signaling	3936S
Goat anti-mouse-HRP	Sigma	A0168
Goat anti-Rabbit-HRP	Sigma	A0545
Bacterial and Virus Strains		
Escherichia coli Top10	Widely available	N/A
Escherichia coli BL21	Widely available	N/A
Escherichia coli BL21 LamP	[35]	N/A

Agrobacterium tumefaciens GV3101	Widely available	N/A
Recombinant Proteins and Peptides		
His_6-MpCPK28	This study.	N/A
His_6-MpCPK28^{K128E}	This study.	N/A
MBP-MpPBLa	This study.	N/A
MBP-MpPBLa^{D228N}	This study.	N/A
GST-MpPUB20a	This study.	N/A
GST-MpPUB20c	This study.	N/A
GST-MpPUB20d	This study.	N/A
GST-MpPUB20e	This study.	N/A
GST-MpPUB20g	This study.	N/A
GST-AtBIK1	This study.	N/A
GST-AtBIK1$^{K105A/K106A}$	This study.	N/A
His-UBA1	This study.	N/A
His-UBC8	This study.	N/A
His-UBC30	This study.	N/A

rhHA-Ubiquitin	R&D Systems	U110
Calmodulin (Petunia isoform CaM81)	[49]	Gift from Wayne Snedden, Queen's University
Elf18 [SKEKFERTKPHVNGTIG]	EZBiolab	N/A (custom)
AtPep1 [ATKVKAKQRGKEKVSSGRPGQHN]	EZBiolab	N/A (custom)
Critical Commercial Assays and Reagents		
pIMAGO HRP Detection on Western Blot	Tymora Analytical	800-40
Phospho-tag Gel Stain	APB Bio	P005A
Presto Mini Plasmid Kit	GeneAid	PDF100
GenepHlow Gel/PCR Kit	GeneAid	DFH300
LR Clonase II	Invitrogen	11791020
Gibson Assembly Mastermix	New England Biolabs	E2611
All restriction enzymes and T4 ligase	New England Biolabs	Widely available
In-Fusion kit	Takara	638947
Q5 *Taq* Polymerase	New England Biolabs	M0491
Direct-zol RNA MiniPrep Zymo Kit	Ozyme	R2052

DNAse RQ	Promega	M6101
M-MLV Reverse Transcriptase Kit	Promega	M1701
Light Cycler 480 SYBR Green I Master Mix	Roche	04707516001
HisPur™ Ni-NTA resin	Thermo Fisher Scientific	25215
Glutathione agarose beads	Sigma Aldrich	G4510
Amicon centrifugal Ultra-15 filter units	Millipore Sigma	30 kDa MWCO (UFC903024); 50 kDa MWCO (UFC905024)
Amicon centrifugal Ultra-4 filter units	Millipore Sigma	30 kDa MWCO (UFC803024); 50 kDa MWCO (UFC805024)
Colloidal Chitin polysaccharide	Elicityl	GLU411
ECL Clarity Substrate	Bio-Rad	1705061
Polyvinylidene difluoride (PVDF) membranes	Bio-Rad	1620177
Coomassie Brilliant Blue (CBB R-250)	Schwarz/Mann Biotech	821616
SimplyBlue SafeStain (CBB G-250)	Invitrogen	46-5044

SynaptoRed™ Reagent (FM464)	Calbiochem	574799-5MG
Miracloth	Calbiochem	475855-1R
Trypsin	Promega	V5113
Triethylammonium Bicarbonate (TEAB)	Sigma	T7408
Experimental Models: Organisms/Strains		
Arabidopsis thaliana Col-0	N/A	N/A
A. thaliana (Col-0) *cpk28-1*	[11,12]	GABIKAT_532308
A. thaliana (Col-0) *cpk28-1 /35S:AtCPK28-YFP*	[11,12]	N/A
A. thaliana (Col-0) *cpk28-1 /35S:MpCPK28-GFP line 5-8*	This study; **Table S1.**	N/A
A. thaliana (Col-0) *cpk28-1 /35S:MpCPK28^{K128E}-GFP line 12-2*	This study; **Table S1.**	N/A
Marchantia polymorpha Takaragaike-1 (Tak-1)	[50]	N/A
M. polymorpha (Tak-1) *MpCPK28-OE2*	This study; **Table S1.**	N/A
Oligonucleotides		
See **Table S1.**	See **Table S1**.	N/A

Recombinant DNA		
p50507-MpoEF1pro:MpCPK28	This study; **Table S1.**	N/A
pENTR-MpCPK28 (no promoter, no stop codon)	This study; **Table S1.**	N/A
pENTR-MpCPK28^{K128E} (no promoter, no stop codon)	This study; **Table S1.**	N/A
pK7FWG2-p35S:MpCPK28-GFP	This study; **Table S1.**	N/A
pK7FWG2-p35S:MpCPK28^{K128E}-GFP	This study; **Table S1.**	N/A
pET28a+-pT7:His$_6$-MpCPK28	This study; **Table S1.**	N/A
pET28a+-pT7:His$_6$-MpCPK28^{K128E}	This study; **Table S1.**	N/A
pOPINM-pT7:MBP-His$_6$-MpPBLa	This study; **Table S1.**	N/A
pOPINM-pT7:MBP-His$_6$-MpPBLa^{D228N}	This study; **Table S1.**	N/A
pENTR-MpPBLa (no promoter, no stop codon)	This study; **Table S1.**	N/A
pK7FWG2-p35S:MpPBLa-GFP	This study; **Table S1.**	N/A
pGex6p.1-pT7:GST-MpPUB20a	This study; **Table S1.**	N/A
pGex6p.1-pT7:GST-MpPUB20c	This study; **Table S1.**	N/A
pGex6p.1-pT7:GST-MpPUB20d	This study; **Table S1.**	N/A

pGex6p.1-pT7:GST-MpPUB20e	This study; **Table S1.**	N/A
pGex6p.1-pT7:GST-MpPUB20g	This study; **Table S1.**	N/A
pGex6p.1-pT7:GST-AtBIK1	[26]	N/A
pGex6p.1-pT7:GST-AtBIK1$^{K105A/K106A}$	[26]	N/A
pDEST17-pT7:His$_6$-AtUBA1	[48]	N/A
pDEST17-pT7:His$_6$-AtUBC8	[48]	N/A
pDEST17-pT7:His$_6$-AtUBC30	[48]	N/A
Software and Algorithms		
Prism	GraphPad	v10
IQ-TREE	[51]	v2.0.3 and v2.3.4
FastTree	[65]	v2.1.10
MAFFT	[52]	v7.490 and v7.471
TrimAl	[53]	v1.4.rev15
HMMER	hmmer.org	v3.4
ModelFinder	[54]	N/A
Blast+	NCBI	v2.11.0+ and

		v2.12.0+ds-3build1
iTOL	[55]	v6 and v5
ImageLab	Bio-Rad	v6.1
MarpolBase	[56]	N/A
WebLogo	[57]	v3
Phosphoproteomics	MaxQuant	v2.0.3.0
Deposited data		
Phosphoproteomics data	This study	PRIDE PXD056365

381

382 ## Contact for Reagent and Resource Sharing

383 Further information and requests for resources and reagents should be directed to and
384 will be fulfilled by the Lead Contact, Jacqueline Monaghan
385 (jacqueline.monaghan@queensu.ca).

386

387 ## Experimental Model and Subject Details

388 ***Arabidopsis thaliana:*** *A. thaliana* plants (ecotype Col-0) were grown in controlled
389 environment chambers (BioChambers and Conviron) in the Queen's University
390 Phytotron. For soil assays, seeds were sown on Sunshine Mix 1 (Sungro) and seedlings
391 transplanted to larger pots about a week after germination. Plants were grown under
392 short-day conditions (8h light; 150 μM photons m^2 s^{-1}) at 22°C, watered when needed

393 and supplemented with 1g/L fertilizer (20N:20P:20K) every 2 weeks. Mite bags containing
394 *Amblyseius swirskii* (Koppert) were added to each tray of plants bi-weekly to prevent pest
395 infestations. Elf18-induced ROS burst assays were performed on 4- to 5-week-old plants
396 as described in [58]. At the time of vegetative-to-reproductive transition (~6 weeks), plants
397 were transferred to a chamber under long-day conditions (14h light) to assess stem
398 elongation. For plate assays, seeds were surface-sterilized with 40% bleach for 30
399 minutes, rinsed well with sterile water, stratified in the dark at 4°C for 2-5 days, and sown
400 on petri plates containing 0.5X Murashige & Skoog (MS) media and 0.8% agar. To assess
401 growth inhibition, 4-day-old seedlings were transferred to single wells of 48-well plates
402 containing liquid 0.5X MS media supplemented with 1% sucrose and the indicated
403 concentration of AtPep1. After 12 days, individual seedlings were blotted dry and weighed
404 on an analytical scale as described in [58]. Transgenic lines were generated by floral dip
405 with *Agrobacterium tumefaciens* GV3101 according to [59]. Bacterial pellets were
406 resuspended in 5% sucrose and 0.01% Silguard as a surfactant to an OD_{600} = 0.5 and
407 applied to unopened buds of ~5-week-old *A. thaliana* plants grown since germination in
408 long-day conditions. Primary stems were trimmed to encourage axillary bud formation.
409 Inoculated plants were kept in the dark overnight and seeds collected several weeks later.
410 T1 plants were selected on 0.5X MS media with 0.8% agar and 50 ug/mL kanamycin prior
411 to soil transfer. Homozygous lines containing single inserts were used for phenotyping,
412 as indicated from segregation analysis in the T2 and T3 generations.

413

414 ***Nicotiana benthamiana:*** *Nicotiana benthamiana* seeds were sown directly on potting
415 soil as above, transplanted as individual seedlings per pot, and grown in a dedicated
416 growth chamber (Conviron) under similar conditions, except with a 16-h-light/8-h-dark
417 cycle and fertilized weekly. Binary vectors were transfected into *Agrobacterium*
418 *tumefaciens* strain GV3101 and transiently expressed in *N. benthamiana* as described in
419 [60].

420

421 ***Marchantia polymorpha:*** *Marchantia polymorpha ssp ruderalis* ecotype Takaragaike-1
422 (Tak-1) was cultivated axenically from gemmae and grown under a long day photoperiod
423 (16 h light at 22°C/8h dark at 20°C), with 60-80 µE light intensity) on 0.5X strength
424 Gamborg B5 medium (Sigma, G5396), pH 5.7, 1.4% Agar-Agar (Sigma, A7921).
425 Gemmae and thalli growth and development was captured using an Axio Zoom.V16
426 (Zeiss), GT-200 scanner (Epson), and analyzed with ImageJ. Transformation was
427 conducted as previously described [61], with some modifications. Freshly collected
428 gemmae from axenic *M. polymorpha* Tak-1 were grown in 0.5X strength Gamborg B5
429 medium for five days. For each transformation, ~30 gemmalings were ground in a sterile,
430 250 mL stainless steel bowl (Waring, USA) in 10 mL of M51C (Takenaka et al., 2000) for
431 30 seconds. The grinded material was then transferred to a 250-mL erlenmeyer flask
432 containing 40 mL of M51C medium and kept shaking (180 rpm) for three days at 22°C
433 16h light/ 20°C 8h dark. To co-culture with *A. tumefaciens* GV3101 for transformation,
434 100 μL of a saturated culture (pellet resuspended in 1 mL of M51C) was supplemented
435 with 100 μM acetosyringone and 500 mg/mL glutamine. After three days, the content of
436 the flasks was transferred into 50 mL conical tubes. Plant tissues were washed by
437 decantation four times with sterile water, and plated on selective media: 0.5X Gamborg
438 B5 with 200 mg/L amoxycilin (Levmentin, Laboratoires Delbert, FR) and 10 mg/L
439 hygromycin (Duchefa Biochimie, FR). Chitin-induced ROS burst assays were performed
440 on 4 week-old thalli as described in [32].

441

442 Method Details

443 Phylogenetics

444 To explore the evolutionary history of CDPKs, we used HMMER v3.4 and HMMscan
445 (hmmer.org) employing the complete PFAM and TIGERFAM datasets to thoroughly
446 examine protein sequences containing a protein kinase (PF00069, TIGR03903) from the
447 genomes of *Selaginella moellendorffii* (GCF_000143415.4), *Physcomitrium patens*

448 (GCF_000002425.4), *Chara braunii* (GCA_003427395.1), *Klebsormidium nitens*
449 (GCA_000708835.1), *Spirogloea muscicola* (GCA_009602725.1), *Oryza sativa*
450 (Japonica Group; GCF_001433935.1), *Amborella tricopoda* (GCF_000471905.2), *Picea*
451 *abies* (V1.0b), and *Marchantia polymorpha* (V6.r1). So that we could include the CRK
452 subfamily, we did not further refine this search with PF00036 but rather compared
453 sequences with an e-value >1.1e-30 to CDPK/CRK orthologs from *Arabidopsis thaliana*
454 (TAIR10) using BLASTp 2.12.0+ to confirm homology (e-value 1e-5 allowing up to 10
455 targets). Five apicomplexan CPKs, including *Toxoplasma gondii* TgCPK1 (ToxoDB ID
456 162.m00001), *Toxoplasma gondii* TgCPK3 (ToxoDB ID 541.m00134), *Plasmodium*
457 *falciparum* PfCPK3 (PlasmoDB ID PFC0420w), *Cryptosporidium parvum* CpCPK1
458 (CryptoDB ID cgd3_920), and *Cryptosporidium parvum* CpCPK3 (CryptoDB ID
459 cgd5_820) were included in the alignments and used as outgroups. In total, 157
460 sequences were aligned using MAFFT v7.490 [52] with the L-INS-i strategy, and sequences
461 were trimmed using TrimAl v1.4.rev15 [53], which was employed for automated alignment
462 trimming and removing poorly aligned sequences. The phylogenetic tree was
463 reconstructed using IQ-TREE v2.3.4 [62], where the best-fitting evolutionary model
464 (Q.plant+R6) was determined using ModelFinder [54] as implemented in IQ-TREE. The
465 tree's robustness was assessed by applying Jackknife resampling with 1000 replicates,
466 in addition to SH-aLRT [63] and UltraFast Bootstraps [64] for branch support, also using 1000
467 replicates. The final maximum likelihood tree was visualized and annotated in iTOL v6 [55].

468

469 To explore the deep evolutionary history of subgroup IV CDPKs, sequences were
470 retrieved from a database containing 193 plant species covering the Viridiplantae diversity
471 using the tBLASTn v2.11.0+ [65] with an e-value threshold of 1-e10. Homolog nucleotide
472 sequences were then aligned using MAFFT v7.471 [52] and the FFT-NS-2 strategy.
473 Subsequent alignment was then trimmed using trimAl v1.4 [53] to remove positions with
474 more than 60% of gaps. Finally, the tree was reconstructed using FastTree v2.1.10 [66] with
475 default parameters and the -gtr option. From this tree, subtree corresponding to orthologs
476 of MpCPK28 was pruned, and sequences aligned and trimmed as described above.

477 Maximum likelihood tree was reconstructed using IQ-TREE v2.0.3 [62] where the best-fitting
478 evolutionary model (GTR+F+R7) was determined using ModelFinder as implemented in
479 IQ-TREE [54] according to the Bayesian Information Criteria (BIC). Branch supports were
480 estimated using 10,000 replicates of both SH-aLRT [63] and UltraFast Bootstraps [64]. Trees
481 were visualized and annotated in iTOL v5 [55].

482

483 Molecular cloning

484 Detailed information about molecular cloning of all vectors used in this study can be found
485 in **Table S1**. We used several molecular cloning methods including Golden Gate,
486 Gateway, In-Fusion, Gibson Assembly, and digestion-ligation cloning. For Golden Gate
487 cloning, coding sequences were domesticated, synthesized and cloned into pMS
488 (GeneArt, Thermo Fisher Scientific), and assembled as described in [61]. For Gateway
489 cloning, recombination of entry vectors into Gateway-compatible binary vectors was
490 achieved using Gateway LR Clonase II (Invitrogen) according to the manufacturer's
491 instructions. Custom synthetic DNA fragments (Twist BioSciences or GeneArt) or PCR
492 amplicons generated using Q5 *Taq* polymerase (NEB) and gene-specific primers, were
493 used for In-Fusion cloning with the In-Fusion Snap Assembly Master Mix (Takara), or for
494 Gibson Assembly using the Gibson Assembly Master Mix (NEB), or for digestion-ligation
495 cloning using construct-specific endonucleases (NEB) and T4 DNA ligase (NEB), all
496 according to the manufacturer's directions. Mutations were incorporated either though
497 PCR-mediated site-directed mutagenesis as described in [12], or at the gene synthesis
498 stage. Plasmids were transfected into *Escherichia coli* Top10 cells for replication and
499 isolated using standard miniprep kits. Successful assembly of all plasmids was verified
500 using Sanger sequencing or whole-plasmid sequencing (Plasmidsaurus).
501

502 ## RNA isolation, cDNA synthesis, and RT-qPCR

503 Total RNA was extracted from ~100 mg of ground frozen tissue from 2-3 weeks old *M.*
504 *polymorpha* thalli using the Direct-zol RNA MiniPrep Zymo Kit (Ozyme) following the
505 manufacturer's instructions. 1 μg of total RNA was treated with DNAse RQ1 (Promega)
506 and cDNA was synthesized using the M-MLV Reverse Transcriptase Kit (Promega), both
507 according to the manufacturer's instructions. Quantitative real-time PCR (RT-qPCR) was
508 performed using 4 μL of 5-fold diluted cDNA, 5 μL of LightCycler 480 SYBR Green I
509 Master Mix (Roche) and 1 μL of each primer at 10 μM, using the CFX Opus 384 Real-
510 Time PCR System (Bio-Rad). Primers used for qPCR have an efficiency between 1.96-
511 2.01 and are provided in **Table S1**.

512

513 ## Recombinant protein purification, *in vitro* kinase assays, and *in vitro* E3
514 ## ligase assays

515 All proteins were expressed and purified from *E. coli* strain BL21 or BL21-λP cells as
516 recently described [60]. His_6-tagged proteins were purified using nickel-nitrilotriacetic acid
517 (HisPur™ Ni-NTA, Thermo Fisher Scientific), and GST-tagged proteins were purified
518 using pre-hydrated glutathione agarose beads (Sigma Aldrich). His_6-tagged proteins were
519 eluted by sequential washes with imidazole-containing buffers at increasing
520 concentrations (10 mM, 25 mM, 50 mM, 250 mM, and 500 mM) and dialyzed overnight
521 at 4°C in 2000 volumes of buffer containing 25 mM Tris-HCl (pH 7.5), 50 mM NaCl, and
522 1 mM DTT. GST-tagged proteins were eluted by incubation at 4°C overnight in a buffer
523 containing 50 mM Tris-HCl (pH 7.5), 10 mM reduced glutathione, and 5 mM DTT. All
524 proteins were concentrated using Amicon Ultra-15 or Ultra-4 centrifugal filter units (30 or
525 50 kDa MWCO; MilliporeSigma), and concentrations were determined using the Bradford
526 assay (Thermo Fisher). Proteins were either immediately used in assays or aliquoted,
527 flash-frozen in liquid N_2 and stored at –80°C until further use.

528

529 *In vitro* kinase assays using pIMAGO (Tymora Analytical) or Phospho-tag gel stain (APB
530 Bio) were performed according to the manufacturer's instructions and as previously
531 described [26]. Ca^{2+}-dependent autophosphorylation assays were performed by incubating
532 5 µg of purified recombinant His_6-MpCPK28 in a 50-µL reaction containing 25 mM Tris-
533 HCl (pH 7.5), 10 mM $MgCl_2$, 1 mM DTT, 100 µM ATP, and either 100 µM $CaCl_2$ or 10 mM
534 EGTA. The reaction was carried out at 30°C for 10 minutes. Reactions were terminated
535 in 5× Laemmli sample buffer (LSB) at 80°C for 10 minutes prior to detection using
536 pIMAGO. To assess CaM-mediated inhibition, 5 µg of His_6-MpCPK28 was incubated in a
537 buffer containing 25 mM Tris-HCl (pH 7.5), 10 mM $MgCl_2$, 1 mM DTT, and 1 mM PMSF,
538 with or without 100 µM $CaCl_2$ or 100 µM ATP, and with or without 2 µM CaM as described
539 previously [35]. The reactions were incubated at 30°C for 30 minutes prior to the addition of
540 100 µM ATP to allow the formation of the MpCPK28-CaM complex. After ATP addition,
541 the reactions proceeded for 30 seconds. Reactions were terminated in 5× LSB at 80°C
542 for 10 minutes prior to detection using pIMAGO. To assess the transphosphorylation
543 between His6-MpCPK28 and MBP-His6-MpPBLa^{D228N}, 2 µg of kinase and 4 µg of
544 substrate were incubated in a 50-*µ*L reaction containing 25 mM Tris (pH 7.5), 10 mM
545 $MgCl_2$, 1 mM DTT, and 1 mM PMSF, with or without 100 *µ*M ATP. The reaction was
546 incubated at 30°C for 60 minutes and terminated in 5× LSB at 80°C for 10 minutes prior
547 to detection using Phospho-tag gel stain. Transphosphorylation assays using γP32-ATP
548 were performed as recently described [60], using 2 µg of kinase and 4 µg of substrate in a
549 buffer containing 50 mM Tris-HCl (pH 8.0), 25 mM $MgCl_2$, 500uM $CaCl_2$, 5 mM DTT, 5
550 µM ATP, and 2-4 µCi γ-[P32]-ATP, and incubated at 30˚C for 10 minutes. Reactions were
551 terminated in 5× LSB at 80°C for 10 minutes, separated by SDS-PAGE. The resulting
552 gels were sandwiched between two sheets of transparency film, exposed to a storage
553 phosphor screen (Molecular Dynamics), and visualized using a Typhoon 8600 Imager
554 (Molecular Dynamics). Gels were post-stained with Coomassie Brilliant Blue (CBB) R-
555 250 (MP Biomedicals) or SimplyBlue SafeStain (Invitrogen; CBB G-250) and scanned.

556

557 *In vitro* E3 ubiquitin ligase assays were performed by incubating 2 µg of recombinant
558 GST-MpPUB20e and 75 µg/mL of HA-tagged ubiquitin (R&D Systems) in a buffer
559 containing 25 mM Tris-HCl (pH 7.4), 5 mM $MgCl_2$, 25 mM KCl, 0.33 mM DTT, 1.5 mM
560 ATP, 4 ng/µL E1 (UBA1), and 9 ng/µL E2 (UBC8 or UBC30). For trans-ubiquitination
561 assays, 2 µg of substrate was additionally added. Reactions were incubated at 30°C for
562 10 - 180 min, terminated in 4× LSB at 80°C for 3 minutes, and finally separated by SDS-
563 PAGE followed by immunoblot.

564

565 Phosphoproteomics

566 Phosphoproteomics was conducted exactly as described in [67] with data searched against
567 the *Marchantia polymorpha* v3.1 proteome available on Phytozome. Proteomics data has
568 been deposited to the ProteomeXchange Consortium via the PRIDE [68]
569 (https://www.ebi.ac.uk/pride/) partner repository with the data set identifier PXD056365.
570 Username: reviewer_pxd056365@ebi.ac.uk; Password: w9uEckCrRqPJ.

571

572 Cell-free degradation assays

573 Tissue from Arabidopsis (4- to 5-week-old healthy mid-layer leaves from plants grown on
574 soil) and Marchantia (3- to 4-week-old plants grown on ½ B5 medium) plants was
575 collected and ground to a fine powder in liquid N_2. Total protein was extracted in a buffer
576 containing 50 mM Tris-MES (pH 8.0), 0.5 M sucrose, 10 mM EDTA (pH 7.5 or 8.0), 5 mM
577 DTT, and 1 mM $MgCl_2$ at a ratio of approximately 1 mL buffer per ~1 mL ground tissue.
578 The mixture was incubated at 4°C with shaking for 1-1.5 hours, followed by centrifugation
579 at 14,000 × *g* for 30 minutes at 4°C. The supernatant was filtered through miracloth to
580 remove any remaining plant matter. Protein concentration was determined using a
581 Bradford assay (Thermo Fisher), and the extract was normalized to 1.0 mg/mL. For the
582 degradation assay, 1.0 mg/mL of freshly extracted protein was mixed with 1 µL of 1.5
583 mg/mL recombinant BIK1 proteins and 10 mM ATP in a 400 µL reaction incubated at

584 30°C. If MG132 proteasome inhibitor was used, a 50 μL sample was taken at 0 hour,
585 mixed with 0.5 μL of 10 mM MG132, and the reaction was stopped at 6 hours. A 50-µL
586 sample was taken every 2 hours, and the reaction was stopped by adding 5× LSB at 80°C
587 for 10 minutes. The samples were subjected to SDS-PAGE followed by immunoblotting.

588 Immunoblots

589 Proteins were separated by 6-10% SDS-PAGE, transferred onto polyvinylidene difluoride
590 membranes (Bio-Rad), and blocked with 5% nonfat milk or bovine serum albumin (BSA)
591 in Tris-buffered saline containing 0.05–0.1% Tween-20. All antibodies used are listed in
592 the **Key Resources Table**. Membranes were incubated with ECL Clarity Substrate (Bio-
593 Rad), visualized on a ChemiDoc Touch Imaging System (Bio-Rad) and subsequently
594 stained with Coomassie Brilliant Blue (CBB) R-250 (MP Biomedicals) as a loading control.

595

596 Confocal microscopy

597 Images were taken using a Zeiss LSM710 confocal microscope in the Biology Department
598 at Queen's University and processed using Zeiss Zen Software. Roots of Arabidopsis
599 seedlings were stained with 2 µM FM464 (Calbiochem) prior to mounting in water on a
600 glass slide. *N. benthamiana* leaf samples were collected with a 4-mm biopsy punch and
601 mounted abaxial-side-up on a glass slide in a drop of water. For localization of MpPBLa-
602 GFP, we co-expressed BRI1-mRFP (Saile et al., 2021). Fluorescent proteins were excited
603 with a 488 nm Argon laser and imaged using separate channels to detect emission of
604 GFP (510-540 nm) or RFP (635-680 nm).

605

606 Quantification and Statistical Analyses

607 Data were graphed using GraphPad Prism v10. Parameters for all statistical tests are
608 described in the figure legends.

Accession numbers

Mp4g01600/Mapoly0098s0040//MpCPK28;

Mp3g25360/Mapoly0100s0049/MpPBLa;

Mp3g01700/Mapoly0007s0162/MpPUB20a;

Mp3g22750/Mapoly0024s0052/MpPUB20b;

Mp3g22740/Mapoly0024s0051/MpPUB20c;

Mp3g11730/Mapoly0037s0024/MpPUB20d;

Mp7g11020/Mapoly0003s0116/MpPUB20e;

Mp2g06090/Mapoly0021s0064/MpPUB20f;

Mp7g11000/Mapoly0003s0114/MpPUB20g.

References

1. Yip Delormel, T., and Boudsocq, M. (2019). Properties and functions of calcium-dependent protein kinases and their relatives in Arabidopsis thaliana. New Phytol. *224*, 585–604.

2. Hu, Z., Li, J., Ding, S., Cheng, F., Li, X., Jiang, Y., Yu, J., Foyer, C.H., and Shi, K. (2021). The protein kinase CPK28 phosphorylates ascorbate peroxidase and enhances thermotolerance in tomato. Plant Physiol. *186*, 1302–1317.

3. Ding, S., Lv, J., Hu, Z., Wang, J., Wang, P., Yu, J., Foyer, C.H., and Shi, K. (2022). Phytosulfokine peptide optimizes plant growth and defense via glutamine synthetase GS2 phosphorylation in tomato. EMBO J., e111858.

4. Wang, J., Wang, S., Hu, K., Yang, J., Xin, X., Zhou, W., Fan, J., Cui, F., Mou, B., Zhang, S., et al. (2018). The Kinase OsCPK4 Regulates a Buffering Mechanism That Fine-Tunes Innate Immunity. Plant Physiol. *176*, 1835–1849.

5. Bundó, M., and Coca, M. (2016). Enhancing blast disease resistance by overexpression of the calcium-dependent protein kinase OsCPK4 in rice. Plant Biotechnol. J. *14*, 1357–1367.

635 6. Campos-Soriano, L., Gómez-Ariza, J., Bonfante, P., and San Segundo, B. (2011). A rice
636 calcium-dependent protein kinase is expressed in cortical root cells during the presymbiotic
637 phase of the arbuscular mycorrhizal symbiosis. BMC Plant Biol. *11*, 90.

638 7. Li, H., Zhang, Y., Wu, C., Bi, J., Chen, Y., Jiang, C., Cui, M., Chen, Y., Hou, X., Yuan, M.,
639 et al. (2022). Fine-tuning OsCPK18/OsCPK4 activity via genome editing of phosphorylation
640 motif improves rice yield and immunity. Plant Biotechnol. J. *20*, 2258–2271.

641 8. Wu, Y., Zhang, L., Zhou, J., Zhang, X., Feng, Z., Wei, F., Zhao, L., Zhang, Y., Feng, H.,
642 and Zhu, H. (2021). Calcium-Dependent Protein Kinase GhCDPK28 Was Dentified and
643 Involved in Verticillium Wilt Resistance in Cotton. Front. Plant Sci. *12*, 772649.

644 9. Gao, S., Shao, W., Wu, J., Zhao, Z., Hu, W., Shao, P., Hua, J., Zou, B., and Huang, Q.
645 (2024). GhCPK28 negatively regulates the immune response by phosphorylating
646 GhTIFY3b. bioRxiv, 2024.02.23.581816. https://doi.org/10.1101/2024.02.23.581816.

647 10. Wang, F., Liang, S., Wang, G., Hu, T., Fu, C., Wang, Q., Xu, Z., Fan, Y., Che, L., Min, L., et
648 al. (2024). CRISPR-Cas9-mediated construction of a cotton CDPK mutant library for
649 identification of insect-resistance genes. Plant Commun. *0*, 101047.

650 11. Matschi, S., Werner, S., Schulze, W.X., Legen, J., Hilger, H.H., and Romeis, T. (2013).
651 Function of calcium-dependent protein kinase CPK28 of Arabidopsis thaliana in plant stem
652 elongation and vascular development. Plant J. *73*, 883–896.

653 12. Monaghan, J., Matschi, S., Shorinola, O., Rovenich, H., Matei, A., Segonzac, C.,
654 Malinovsky, F.G., Rathjen, J.P., MacLean, D., Romeis, T., et al. (2014). The calcium-
655 dependent protein kinase CPK28 buffers plant immunity and regulates BIK1 turnover. Cell
656 Host Microbe *16*, 605–615.

657 13. Matschi, S., Hake, K., Herde, M., Hause, B., and Romeis, T. (2015). The calcium-
658 dependent protein kinase CPK28 regulates development by inducing growth phase-
659 specific, spatially restricted alterations in jasmonic acid levels independent of defense
660 responses in Arabidopsis. Plant Cell *27*, 591–606.

661 14. Monaghan, J., Matschi, S., Romeis, T., and Zipfel, C. (2015). The calcium-dependent
662 protein kinase CPK28 negatively regulates the BIK1-mediated PAMP-induced calcium
663 burst. Plant Signal. Behav. *10*, e1018497.

664 15. Sowders, J.M., Jewell, J.B., and Tanaka, K. (2024). CPK28 is a modulator of purinergic
665 signaling in plant growth and defense. Plant J. https://doi.org/10.1111/tpj.16656.

666 16. Ding, Y., Yang, H., Wu, S., Fu, D., Li, M., Gong, Z., and Yang, S. (2022). CPK28-NLP7
667 module integrates cold-induced Ca^{2+} signal and transcriptional reprogramming in
668 *Arabidopsis*. Sci Adv *8*, eabn7901.

669 17. Zhu, X., Wang, F., Li, S., Feng, Y., Yang, J., Zhang, N., and Si, H. (2022). Calcium-
670 Dependent Protein Kinase 28 Maintains Potato Photosynthesis and Its Tolerance under
671 Water Deficiency and Osmotic Stress. Int. J. Mol. Sci. *23*.
672 https://doi.org/10.3390/ijms23158795.

673 18. Wang, J., Grubb, L.E., Wang, J., Liang, X., Li, L., Gao, C., Ma, M., Feng, F., Li, M., Li, L., et

674 al. (2018). A Regulatory Module Controlling Homeostasis of a Plant Immune Kinase. Mol.
675 Cell *69*, 493–504.e6.

676 19. Gonçalves Dias, M., Soleimani, F., and Monaghan, J. (2022). Activation and turnover of the
677 plant immune signaling kinase BIK1: a fine balance. Essays Biochem. *66*, 207–218.

678 20. Bowman, J.L., Arteaga-Vazquez, M., Berger, F., Briginshaw, L.N., Carella, P., Aguilar-Cruz,
679 A., Davies, K.M., Dierschke, T., Dolan, L., Dorantes-Acosta, A.E., et al. (2022). The
680 renaissance and enlightenment of Marchantia as a model system. Plant Cell *34*, 3512–
681 3542.

682 21. Billker, O., Lourido, S., and Sibley, L.D. (2009). Calcium-dependent signaling and kinases
683 in apicomplexan parasites. Cell Host Microbe *5*, 612–622.

684 22. Brawley, S.H., Blouin, N.A., Ficko-Blean, E., Wheeler, G.L., Lohr, M., Goodson, H.V.,
685 Jenkins, J.W., Blaby-Haas, C.E., Helliwell, K.E., Chan, C.X., et al. (2017). Insights into the
686 red algae and eukaryotic evolution from the genome of Porphyra umbilicalis
687 (Bangiophyceae, Rhodophyta). Proc. Natl. Acad. Sci. U. S. A. *114*, E6361–E6370.

688 23. Valmonte, G.R., Arthur, K., Higgins, C.M., and MacDiarmid, R.M. (2014). Calcium-
689 dependent protein kinases in plants: evolution, expression and function. Plant Cell Physiol.
690 *55*, 551–569.

691 24. Wang, J.-P., Xu, Y.-P., Munyampundu, J.-P., Liu, T.-Y., and Cai, X.-Z. (2016). Calcium-
692 dependent protein kinase (CDPK) and CDPK-related kinase (CRK) gene families in tomato:
693 genome-wide identification and functional analyses in disease resistance. Mol. Genet.
694 Genomics *291*, 661–676.

695 25. Jin, Y., Ye, N., Zhu, F., Li, H., Wang, J., Jiang, L., and Zhang, J. (2017). Calcium-
696 dependent protein kinase CPK28 targets the methionine adenosyltransferases for
697 degradation by the 26S proteasome and affects ethylene biosynthesis and lignin deposition
698 in Arabidopsis. Plant J. *90*, 304–318.

699 26. Bredow, M., Bender, K.W., Johnson Dingee, A., Holmes, D.R., Thomson, A., Ciren, D.,
700 Tanney, C.A.S., Dunning, K.E., Trujillo, M., Huber, S.C., et al. (2021). Phosphorylation-
701 dependent subfunctionalization of the calcium-dependent protein kinase CPK28. Proc. Natl.
702 Acad. Sci. U. S. A. *118*. https://doi.org/10.1073/pnas.2024272118.

703 27. Liu, X., Zhou, Y., Du, M., Liang, X., Fan, F., Huang, G., Zou, Y., Bai, J., and Lu, D. (2022).
704 The calcium-dependent protein kinase CPK28 is targeted by the ubiquitin ligases ATL31
705 and ATL6 for proteasome-mediated degradation to fine-tune immune signaling in
706 Arabidopsis. Plant Cell *34*, 679–697.

707 28. Dressano, K., Weckwerth, P.R., Poretsky, E., Takahashi, Y., Villarreal, C., Shen, Z.,
708 Schroeder, J.I., Briggs, S.P., and Huffaker, A. (2020). Dynamic regulation of Pep-induced
709 immunity through post-translational control of defence transcript splicing. Nat Plants *6*,
710 1008–1019.

711 29. Medina-Puche, L., Tan, H., Dogra, V., Wu, M., Rosas-Diaz, T., Wang, L., Ding, X., Zhang,
712 D., Fu, X., Kim, C., et al. (2020). A Defense Pathway Linking Plasma Membrane and

713 Chloroplasts and Co-opted by Pathogens. Cell *182*, 1109–1124.e25.

714 30. Yotsui, I., Matsui, H., Miyauchi, S., Iwakawa, H., Melkonian, K., Schlüter, T., Michavila, S.,
715 Kanazawa, T., Nomura, Y., Stolze, S.C., et al. (2023). LysM-mediated signaling in
716 Marchantia polymorpha highlights the conservation of pattern-triggered immunity in land
717 plants. Curr. Biol. *33*, 3732–3746.e8.

718 31. DeFalco, T.A., and Zipfel, C. (2021). Molecular mechanisms of early plant pattern-triggered
719 immune signaling. Mol. Cell *81*, 4346.

720 32. Chu, J., Monte, I., DeFalco, T.A., Köster, P., Derbyshire, P., Menke, F.L.H., and Zipfel, C.
721 (2023). Conservation of the PBL-RBOH immune module in land plants. Curr. Biol. *33*,
722 1130–1137.e5.

723 33. Kadota, Y., Sklenar, J., Derbyshire, P., Stransfeld, L., Asai, S., Ntoukakis, V., Jones, J.D.,
724 Shirasu, K., Menke, F., Jones, A., et al. (2014). Direct regulation of the NADPH oxidase
725 RBOHD by the PRR-associated kinase BIK1 during plant immunity. Mol. Cell *54*, 43–55.

726 34. Chen, F., Zhang, L., and Cheng, Z.-M.M. (2017). The calmodulin fused kinase novel gene
727 family is the major system in plants converting Ca2+ signals to protein phosphorylation
728 responses. Sci. Rep. *7*, 4127.

729 35. Bender, K.W., Blackburn, R.K., Monaghan, J., Derbyshire, P., Menke, F.L.H., Zipfel, C.,
730 Goshe, M.B., Zielinski, R.E., and Huber, S.C. (2017). Autophosphorylation-based Calcium
731 (Ca2+) Sensitivity Priming and Ca2+/Calmodulin Inhibition of Arabidopsis thaliana Ca2+-
732 dependent Protein Kinase 28 (CPK28). J. Biol. Chem. *292*, 3988–4002.

733 36. Liese, A., and Romeis, T. (2013). Biochemical regulation of in vivo function of plant
734 calcium-dependent protein kinases (CDPK). Biochim. Biophys. Acta *1833*, 1582–1589.

735 37. Trenner, J., Monaghan, J., Saeed, B., Quint, M., Shabek, N., and Trujillo, M. (2022).
736 Evolution and Functions of Plant U-Box Proteins: From Protein Quality Control to Signaling.
737 Annu. Rev. Plant Biol. https://doi.org/10.1146/annurev-arplant-102720-012310.

738 38. Yi, S.Y., Nekrasov, V., Ichimura, K., Kang, S.-Y., and Shirasu, K. (2024). Plant U-box E3
739 ligases PUB20 and PUB21 negatively regulate pattern-triggered immunity in Arabidopsis.
740 Plant Mol. Biol. *114*, 7.

741 39. Trujillo, M., Ichimura, K., Casais, C., and Shirasu, K. (2008). Negative regulation of PAMP-
742 triggered immunity by an E3 ubiquitin ligase triplet in Arabidopsis. Curr. Biol. *18*, 1396–
743 1401.

744 40. Furlan, G., Nakagami, H., Eschen-Lippold, L., Jiang, X., Majovsky, P., Kowarschik, K.,
745 Hoehenwarter, W., Lee, J., and Trujillo, M. (2017). Changes in PUB22 ubiquitination modes
746 triggered by MITOGEN-ACTIVATED PROTEIN KINASE3 dampen the immune response.
747 Plant Cell *29*, 726–745.

748 41. Monaghan, J. (2018). Conserved Degradation of Orthologous RLCKs Regulates Immune
749 Homeostasis. Trends Plant Sci. *23*, 554–557.

750 42. Zhou, X., Wang, J., Peng, C., Zhu, X., Yin, J., Li, W., He, M., Wang, J., Chern, M., Yuan,

751 C., et al. (2016). Four receptor-like cytoplasmic kinases regulate development and
752 immunity in rice. Plant Cell Environ. *39*, 1381–1392.

753 43. Ao, Y., Li, Z., Feng, D., Xiong, F., Liu, J., Li, J.-F., Wang, M., Wang, J., Liu, B., and Wang,
754 H.-B. (2014). OsCERK1 and OsRLCK176 play important roles in peptidoglycan and chitin
755 signaling in rice innate immunity. Plant J. *80*, 1072–1084.

756 44. Zhang, J., Li, W., Xiang, T., Liu, Z., Laluk, K., Ding, X., Zou, Y., Gao, M., Zhang, X., Chen,
757 S., et al. (2010). Receptor-like Cytoplasmic Kinases Integrate Signaling from Multiple Plant
758 Immune Receptors and Are Targeted by a Pseudomonas syringae Effector. Cell Host
759 Microbe *7*, 290–301.

760 45. Lu, D., Wu, S., Gao, X., Zhang, Y., Shan, L., and He, P. (2010). A receptor-like cytoplasmic
761 kinase, BIK1, associates with a flagellin receptor complex to initiate plant innate immunity.
762 Proc. Natl. Acad. Sci. U. S. A. *107*, 496–501.

763 46. Veronese, P., Nakagami, H., Bluhm, B., Abuqamar, S., Chen, X., Salmeron, J., Dietrich,
764 R.A., Hirt, H., and Mengiste, T. (2006). The membrane-anchored BOTRYTIS-INDUCED
765 KINASE1 plays distinct roles in Arabidopsis resistance to necrotrophic and biotrophic
766 pathogens. Plant Cell *18*, 257–273.

767 47. Newcombe, E.A., Delaforge, E., Hartmann-Petersen, R., Skriver, K., and Kragelund, B.B.
768 (2022). How phosphorylation impacts intrinsically disordered proteins and their function.
769 Essays Biochem. *66*, 901–913.

770 48. Turek, I., Tischer, N., Lassig, R., and Trujillo, M. (2018). Multi-tiered pairing selectivity
771 between E2 ubiquitin-conjugating enzymes and E3 ligases. J. Biol. Chem. *293*, 16324–
772 16336.

773 49. Chiasson, D., Ekengren, S.K., Martin, G.B., Dobney, S.L., and Snedden, W.A. (2005).
774 Calmodulin-like proteins from Arabidopsis and tomato are involved in host defense against
775 Pseudomonas syringae pv. tomato. Plant Mol. Biol. *58*, 887–897.

776 50. Bowman, J.L., Kohchi, T., Yamato, K.T., Jenkins, J., Shu, S., Ishizaki, K., Yamaoka, S.,
777 Nishihama, R., Nakamura, Y., Berger, F., et al. (2017). Insights into Land Plant Evolution
778 Garnered from the Marchantia polymorpha Genome. Cell *171*, 287–304.e15.

779 51. Nguyen, L.-T., Schmidt, H.A., von Haeseler, A., and Minh, B.Q. (2015). IQ-TREE: a fast
780 and effective stochastic algorithm for estimating maximum-likelihood phylogenies. Mol. Biol.
781 Evol. *32*, 268–274.

782 52. Katoh, K., and Standley, D.M. (2013). MAFFT multiple sequence alignment software
783 version 7: improvements in performance and usability. Mol. Biol. Evol. *30*, 772–780.

784 53. Capella-Gutiérrez, S., Silla-Martínez, J.M., and Gabaldón, T. (2009). trimAl: a tool for
785 automated alignment trimming in large-scale phylogenetic analyses. Bioinformatics *25*,
786 1972–1973.

787 54. Kalyaanamoorthy, S., Minh, B.Q., Wong, T.K.F., von Haeseler, A., and Jermiin, L.S. (2017).
788 ModelFinder: fast model selection for accurate phylogenetic estimates. Nat. Methods *14*,
789 587–589.

790 55. Letunic, I., and Bork, P. (2021). Interactive Tree Of Life (iTOL) v5: an online tool for
791 phylogenetic tree display and annotation. Nucleic Acids Res. *49*, W293–W296.

792 56. Kawamura, S., Romani, F., Yagura, M., Mochizuki, T., Sakamoto, M., Yamaoka, S.,
793 Nishihama, R., Nakamura, Y., Yamato, K.T., Bowman, J.L., et al. (2022). MarpolBase
794 Expression: A web-based, comprehensive platform for visualization and analysis of
795 transcriptomes in the liverwort Marchantia polymorpha. Plant Cell Physiol. *63*, 1745–1755.

796 57. Crooks, G.E., Hon, G., Chandonia, J.-M., and Brenner, S.E. (2004). WebLogo: a sequence
797 logo generator. Genome Res. *14*, 1188–1190.

798 58. Bredow, M., Sementchoukova, I., Siegel, K., and Monaghan, J. (2019). Pattern-Triggered
799 Oxidative Burst and Seedling Growth Inhibition Assays in Arabidopsis thaliana. J. Vis. Exp.
800 https://doi.org/10.3791/59437.

801 59. Clough, S.J., and Bent, A.F. (1998). Floral dip: a simplified method for Agrobacterium-
802 mediated transformation of Arabidopsis thaliana. Plant J. *16*, 735–743.

803 60. Dias, M.G., Doss, B., Rawat, A., Siegel, K.R., Mahathanthrige, T., Sklenar, J., Derbyshire,
804 P., Dharmasena, T., Cameron, E., Zipfel, C., et al. (2023). Subfamily C7 Raf-like kinases
805 MRK1, RAF26, and RAF39 regulate immune homeostasis and stomatal opening in
806 Arabidopsis thaliana. bioRxiv, 2023.11.29.569073.
807 https://doi.org/10.1101/2023.11.29.569073.

808 61. Rich, M.K., Vigneron, N., Libourel, C., Keller, J., Xue, L., Hajheidari, M., Radhakrishnan,
809 G.V., Le Ru, A., Diop, S.I., Potente, G., et al. (2021). Lipid exchanges drove the evolution of
810 mutualism during plant terrestrialization. Science *372*, 864–868.

811 62. Minh, B.Q., Schmidt, H.A., Chernomor, O., Schrempf, D., Woodhams, M.D., von Haeseler,
812 A., and Lanfear, R. (2020). IQ-TREE 2: New Models and Efficient Methods for Phylogenetic
813 Inference in the Genomic Era. Mol. Biol. Evol. *37*, 1530–1534.

814 63. Guindon, S., Dufayard, J.-F., Lefort, V., Anisimova, M., Hordijk, W., and Gascuel, O.
815 (2010). New algorithms and methods to estimate maximum-likelihood phylogenies:
816 assessing the performance of PhyML 3.0. Syst. Biol. *59*, 307–321.

817 64. Hoang, D.T., Chernomor, O., von Haeseler, A., Minh, B.Q., and Vinh, L.S. (2018).
818 UFBoot2: Improving the Ultrafast Bootstrap Approximation. Mol. Biol. Evol. *35*, 518–522.

819 65. Camacho, C., Coulouris, G., Avagyan, V., Ma, N., Papadopoulos, J., Bealer, K., and
820 Madden, T.L. (2009). BLAST+: architecture and applications. BMC Bioinformatics *10*, 421.

821 66. Price, M.N., Dehal, P.S., and Arkin, A.P. (2009). FastTree: computing large minimum
822 evolution trees with profiles instead of a distance matrix. Mol. Biol. Evol. *26*, 1641–1650.

823 67. Dias, M.G., Dharmasena, T., Gonzalez-Ferrer, C., Maika, J.E., Gallo, M.C.R., Miguel, V.N.,
824 Dou, R., Bredow, M., Siegel, K.R., Uhrig, R.G., et al. (2024). Catalytically inactive subgroup
825 VIII receptor-like cytoplasmic kinases regulate the immune-triggered oxidative burst in
826 Arabidopsis thaliana. bioRxiv, 2024.05.30.596543.
827 https://doi.org/10.1101/2024.05.30.596543.

68. Perez-Riverol, Y., Csordas, A., Bai, J., Bernal-Llinares, M., Hewapathirana, S., Kundu, D.J., Inuganti, A., Griss, J., Mayer, G., Eisenacher, M., et al. (2019). The PRIDE database and related tools and resources in 2019: improving support for quantification data. Nucleic Acids Res. *47*, D442–D450.

Supplemental Information

Supplemental Table

Provided as a separate spreadsheet.

- **Table S1.** Germplasm, clones, and primers generated in this study.

Supplemental Figures

Provided as a separate PDF.

- **Figure S1.** Phylogenetic tree of CDPKs from various plant lineages.
- **Figure S2.** Phylogenetic tree of subgroup IV CDPKs across the plant lineage.
- **Figure S3.** Genomic and gene expression data for *MpCPK28* and characterization of the *Tak-1/35S:MpCPK28-OE2* transgenic line.
- **Figure S4.** MpPBLa-GFP localizes to the plasma membrane when heterologously expressed in *N. benthamiana*.
- **Figure S5.** Western blot indicating MpCPK28-GFP expression in Arabidopsis transgenic lines.
- **Figure S6.** Identification of MpPUB20 genes in *Marchantia polymorpha*.
- **Figure S7.** Cell-free degradation assays of MpPBLa and AtBIK1 in Col-0 protein extract.
- **Figure S8.** MpPUB20e is capable of auto-ubiquitination in vitro when paired with E2s AtUBC8 or AtUBC30.

Supplemental References